Tunable Energy Absorption in Diatom-inspired Architected Materials Designed for Additive Manufacturing

L. Musenich, L. Derin, A. Stagni, F. Libonati*
University of Genoa, Polytechnic School, Department of Mechanical, Energy, Management and Transportation Engineering, Via all'Opera Pia 15/A, 16145, Genova, Italy

*Corresponding author: flavia.libonati@unige.it

Abstract

Spurred on by additive manufacturing, architected materials have opened up new opportunities to overcome the performance and functionality limitations of commercially available materials. Yet, the development and optimization of this new class of multiscale materials are held back by the intense analytical, computational, and experimental efforts required to understand their complex property-structure-process-performance relationship. To speed up the design process and solve this issue, data-driven approaches are becoming increasingly popular. To demonstrate the potential of metamodeling techniques in materials science, in this study we analyze the mechanical energy absorption properties of honeycombs inspired by diatom frustules. We first generate a dataset through finite element simulations. Then we build regression models that allow us to predict and customize honeycomb features, while minimizing the use of numerical analysis. The combination of Nature's design principles, used to shape biological materials, and metamodeling techniques, applied to in silico testing, represents a powerful opportunity to increase the efficiency and performance of man-made materials, and this research is proof of that.

Keywords

Data-driven material design, bioinspired materials, Diatoms, Finite-element analysis, Metamodeling, Architected Materials, Functional gradients.

Introduction

Architected materials are multiphase lattice materials [1] in which phase connectivity and/or lattice features are carefully controlled on different length scales, through functional gradients and heterogeneities, to ensure the optimal accomplishment of specific functions or properties. Their power lies in the ability to tailor their performance by acting on the interplay between material properties and geometry. Thanks to the many design degrees of freedom they offer, such materials find applications in a multitude of fields such as lightweight structures, wave propagation control, bio-scaffolds, and metamaterials [2]–[4]. Recently, the development of this new class of materials has been mainly driven by the desire to achieve–through engineering processes–the remarkable capabilities observed in biological materials, and composites in particular [5], e.g., the optimal combination of mechanical properties and their amplification with respect to those of the constituent building blocks. Classic examples are bone, wood, and nacre [6]–[11].

The unique performance and multifunctionality of biological materials are attributed to the way natural processes of self-assembly and growth of biomolecules and biominerals (i.e., the biological building blocks [12], [13]) optimize their structures over multiple length scales. Despite the diversity of forms, functions, and properties of materials that can be observed in Nature, they all exhibit common traits. These traits result from the masterful combination of functional regions adapted to local conditions, substructures consisting of subunits with universal chemical constituents/compositions, structural features, gradients, and interfaces [5],

[14]–[19]. The application of this "universality-diversity" paradigm [20]–[22] to the design of architected materials has turned out to be a very promising guide to improve their performances [22]–[26]. In this context, additive manufacturing (AM), thanks to the geometric freedom it provides and to the increasingly wide range of length scales it can cover, is playing a key role on the development of new bioinspired architected materials [2], [3], [26], [27]. Along with AM, advances in imaging, and nanotechnology, combined with developments in computational modeling, have enabled the design of materials with hierarchical structures and complex chemical compositions optimized for specific applications [28], [29]. Besides, structural optimization techniques, well-known to optimize the size, shape, and topology of structures at the macro scale [30], have now become must-use strategies to achieve optimized architectures from the material on.

The intricate property-structure-process-performance relationship (PSPP) of architected materials [31] introduces many complexities that make the multi-scale design and fabrication of architected materials not a straightforward process. Indeed, the development of new architected materials generally involves a trial-and-error approach based on the synergistic use of numerical simulations and experimental tests at different length scales. Given the wide-ranging design degrees of freedom and nonlinearities that characterize these materials, their design development and optimization are highly resource-intensive. In recent years, machine learning (ML), i.e., the use of computer systems that learn to accomplish a given task from data (i.e., to build an analytical model) without being explicitly programmed, has proven to be a valuable method to overcome this issue. Indeed, ML algorithms have been successfully used for the data-driven design of new materials by: (i) guiding the choice of process parameters, (ii) identifying new hierarchical structures, (iii) replacing constitutive equations for the analysis of new material properties, and (iv) improving performance such as fatigue life, buckling resistance, and fracture toughness [32]–[37]. While biomimicry has been successfully used to provide design solutions for materials with superior mechanical properties, ML-based methods have further accelerated the design process and the discovery of new materials.

In this study, we combine Nature design principles with an ML-based material modeling approach to accelerate the design process of new diatom-inspired architected materials with optimized mechanical energy absorption capabilities. Optimized by Nature to survive in very challenging environments, diatoms (i.e., single-celled microalgae widespread in all aquatic environments) represent an impressive model of multifunctionality. Their external siliceous shell, which provides protection from predators' attacks, while controlling nutrient acquisition, diatom sinking rate, light absorption, and acting as a filter against viruses, represents a distinguishing trait that characterizes all observed species. Over the years, what has made diatoms increasingly attractive from a biomimicry perspective is the bio-siliceous exoskeleton that covers them, known as frustule, whose mechanical properties are still poorly understood.

Here, to study the link between the frustule geometry and its energy absorption capabilities, diatom-inspired geometric models are built. Mechanical properties are first calculated through finite element analyses (FEA). Data from FEA is first used to train and validate three common ML regression algorithms, then to build analytical models (i.e., metamodels or surrogate models) that approximate the PSPP relationship of the bioinspired material (predictive analysis). Finally, these metamodels are used to guide the shape optimization of the bioinspired material in order to maximize its energy absorption capacity (prescriptive analysis). This study shows how the joint use of ML algorithms and bio-inspiration significantly accelerates the design process of architected materials, providing a fast and accurate prediction of the FEA outcome.

Materials and Methods

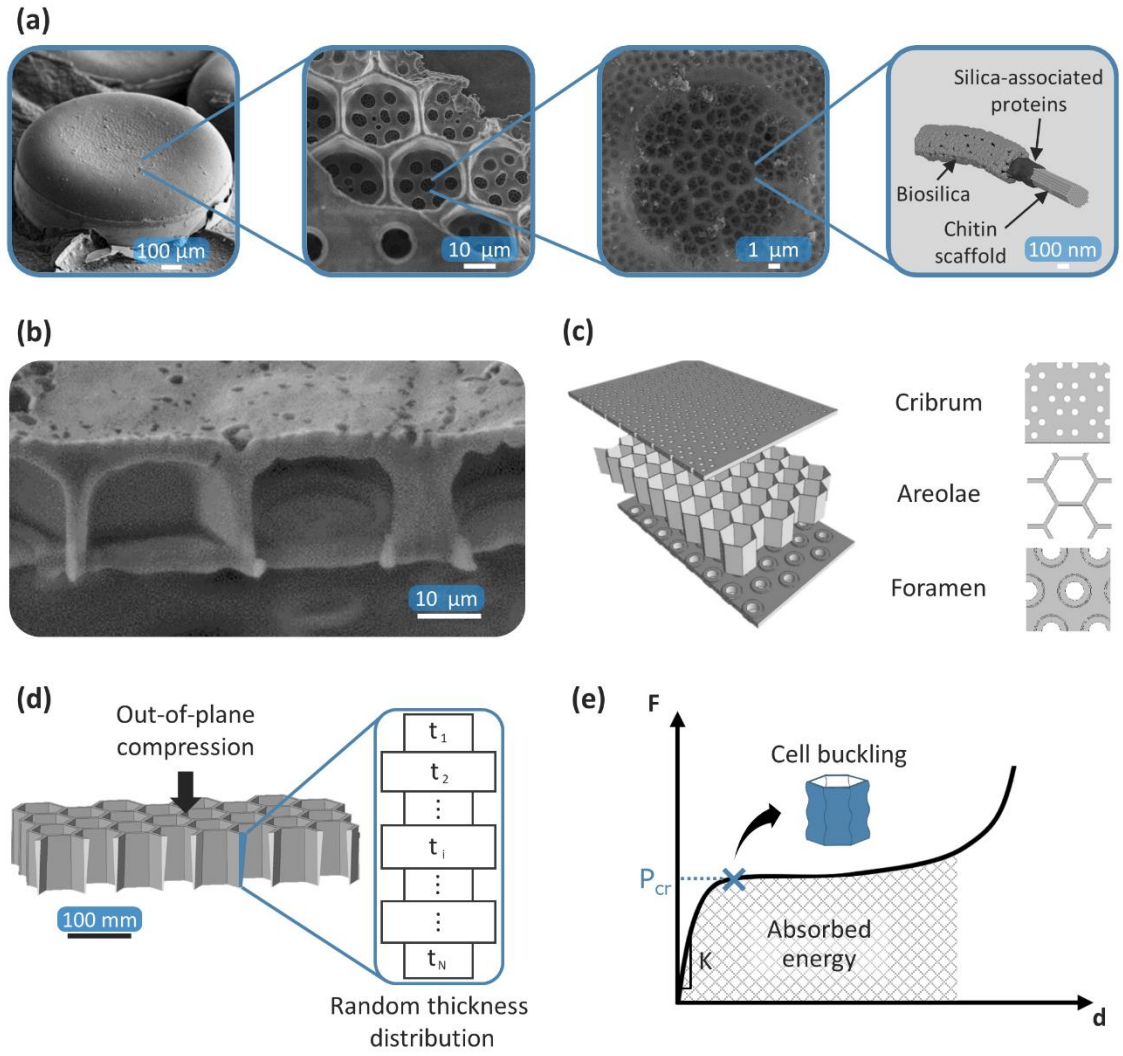

Figure 1 - (a) Hierarchical architecture of the Coscinodiscus diatom frustule with its four different level: "Petri dish" configuration shared by all diatoms (modified from [39], CC BY 4.0); sandwich like structure distinctive for this family of diatoms (modified from [40]); intricate porous network of amorphous silica that covers the entire outer surface of the frustule (modified from [40]); building blocks that make up the frustule (modified from [41], CC BY 4.0). (b) Cross-section of the diatom frustule: view of the thickness gradient present in the areolae cell walls (modified from [39], CC BY 4.0).(c) Simplified geometric model of the sandwich like structure of the Coscinodiscus frustule with its three layers: cribrum, areolae, and foramen. (d) Schematic representation of the analyzed honeycomb like structure with the random thickness distribution. (e) Qualitative representation of the force-displacement diagram of honeycomb structures under out of plane compression.

<u>Biomimetic design approach description</u>

In our work we consider the most widespread species of diatom: the Coscinodiscus. We first perform a geometric analysis, which highlights four different organization levels, depending on the considered length scale (see Figure 1a). Level 2 is the most interesting one from a structural point of view, with its architecture resembling that of sandwich structures. Here we can distinguish three main structural layers (Figure 1b): i) *cribrum*, a first thin layer characterized

by small porosity, ii) *areole*, an intermediate layer with a honeycomb-like topology, and iii) *foramen*, a third layer characterized by the presence of larger holes with respect to those present in the cribrum. We focus our study on the central layer of level 2, the areolae. In fact, it is well known that honeycomb like-structures have been already successfully used in structural as well as in energy absorption application. Thanks to their out-of-plane stiffness and buckling load resistance combined with its lightweight design honeycombs are extremely efficient, especially where weight saving is critical. Diatoms areolae in addition the hexagonal cross section, show different morphological features that positively affect the mechanical properties of the whole structure. More precisely, the areolae layer shows a functional gradient in the wall thickness distribution (Figure 1c). To investigate how the thickness gradient affects the energy absorption capability of the structure, we design a bioinspired model of the diatom honeycomb layer, analyze its behavior under out-of-plane compression, and measure the energy it can absorb.

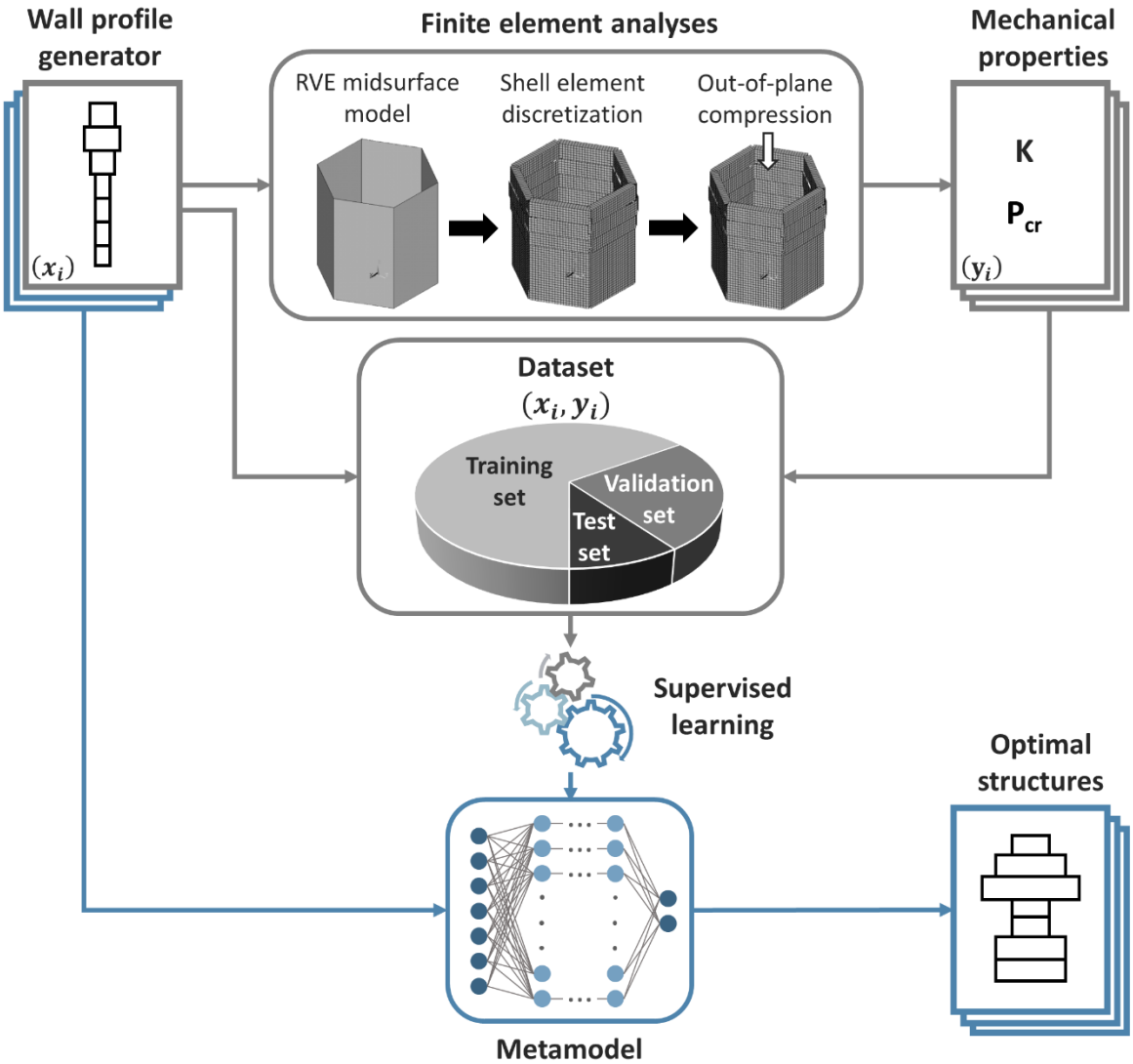

Figure 2 – Representation of the workflow used to train the machine learning algorithms and predicts new structures. The design space was defined by creating seven-components vectors defining the wall thickness distribution. The wall profiles are generated via a Matlab script. Some of the structures are randomly selected and solved via FE analysis to obtain the 2D vector characterizing the absorbed energy: critical buckling load (P_{cr}) and structure stiffness (K). The solved structures are then divided into the training, validation and test set in order to train the ML algorithms. The rest of the structures are used to predict the optimal structure.

Starting from the diatom areolae we create a regular honeycomb structure and, we partition the honeycomb walls into seven segments along the vertical (out-of-plane) axis. Then we assign to each segment a different thickness value in order to replicate the diatom gradient distribution. We choose the thickness values and the hexagon edge length in order to respect the proportions of the natural structure [42]. To limit the number of possible solutions and respect the geometric limitations, each wall partition can be assigned a certain thickness value, selected among five different possible values, which are fixed a priori. This assignment is done through an algorithm that generates a random seven-component vector, where each component represents the thickness value of the hexagonal cell partition. Specific constraints are applied in order to avoid the generation of repetitive structures or unphysical thickness distribution (*i.e.*, zero-thickness). Similar approaches have been already used in literature to address similar problems. To avoid any bias, we also shuffle the order of the generated vectors to have a more homogeneous data set for the ML algorithm training. A schematic representation of the partitioning is depicted in Figure 1d. All the geometries are generated via ANSYS APDL solid modeler. In total, we build 2000 different geometries to be analyzed with the FE software, with the final goal of generating the dataset for the ML algorithms training and validation. The model size is then scaled up with respect to the natural structure, in order to cope with the 3D-printing limitation/accuracy. The geometric size is provided in the Supplementary Information file. Due to the complexity of the problem, to find the optimal thickness distribution within the structure we use an approach that combines FE analysis and ML algorithms. Figure 2 provides a schematic representation of the workflow, which includes four main steps: (i) geometry and parameters definition, (ii) data generation, (iii) ML algorithm definition and training, and (iv) optimal solution prediction.

Finite Element Analysis

The numerical simulations are performed using ANSYS Mechanical APDL. This is crucial for the formulation of customized macros that automatically define the different geometries, material properties and boundary conditions, and analyze the structural behavior. More precisely, the geometry of the bioinspired models is built parametrically, using first-order 3D FE shell-type elements with a mapped mesh. Once the geometry and the partition are defined, an iterative cycle is used to automatically assign the thickness values to each partition, compute the analysis, and save the results into an external data file. We study a total of 2000 different geometries. The honeycomb cells are simulated under uniaxial compressive loading condition. We performed two types of simulations: a linear elastic one, for the evaluation of the structure stiffness (E*), and a linearized buckling analysis, for the evaluation of the critical buckling load (P_{cr}). The combination of E* and P_{cr} provides an estimation of the energy absorption capacity of the structure. Similar approach was also used in previous studies. In fact, the typical response of cellular materials in compression shows an approximate behavior characterized by 3 zones (see Figure1e): (i) linear elastic, (ii) plateau, and (iii) densification. The plateau stress can be approximated with the critical stress, so the dashed area of the plot, representing the absorbed energy, can be seen as a function of E* and P_{cr}. For our purposes, we neglect the densification phase, which has a lower contribution. As boundary conditions, all the lower edge nodes are fixed by constraining their x-, y-, z-displacements, while the upper edge is free. A linear-elastic compression analysis is performed in displacement control, assigning a negative displacement of 0.3 mm to the nodes on the upper edge. For the buckling model the same boundary conditions are adopted but, instead of a displacement, a unitary force is applied. Also, given the large number of simulations, we exploit geometrical symmetry and periodic boundary conditions to limit the computational effort. The material adopted for our simulations is a commercial TPU (Thermoplastic polyurethane), whose mechanical properties are experimentally derived from mechanical testing performed on 3D printed samples. For all the simulations, the material is

considered homogeneous and isotropic. The minimum size of the finite element mesh is defined according to convergence analysis. Before proceeding with all the analysis, an initial validation of the FE model is performed by comparing the results (i.e., E* and P_{cr}) of the constant wall thickness honeycomb with the analytical solution for the honeycomb unit cell, finding a good agreement corresponding to an error between the analytical and numerical results lower than 5%.

Supervised learning

The first step in preparing the metamodels is the definition of the features (*i.e.*, thickness vector) and the definition of the labels. In our case, the labels are the structure stiffness E* and the critical stress P_{cr}, corresponding to critical buckling load P_{cr}, of the analyzed structure. From the whole set of defined geometries, we select 1000 as training set, and 500 as validation set. The training set is used to determine the optimal model parameters while the validation set, which is not used for training, is necessary to estimate the unbiased error of the model, which is fundamental for choosing the optimal model hyperparameters. The remaining data are used as a test set, to assess the error of the optimized model, thus its accuracy [43]. To improve the performances of the meta-models, the labels and features are normalized and centered. This is done because some ML algorithms have a bias on the modulus of the training points. These transformations ensure that all data points are normalized to 1 and have zero mean values, respectively. In this study, we use three different supervised ML approaches to make the regression and find the one that best fits our problem:

1. A linear ridge regression (LRR). Thanks to its high computational efficiency it is always desirable to implement a linear regression as a first approximation [43]. For this meta-model, we use the kernel ridge package from Scikit-learn, with a linear kernel and a value of the regularization parameter *alpha=0.1* in order to avoid eventual underfitting, while overfitting is not a big concern with a low dimensional linear model.
2. A kernel algorithm, in particular the Kernel Ridge Regression (KRR). With Kernel it is possible to capture eventual nonlinearities by maintaining still a good computational efficiency. Thanks to the kernel *trick* the complexity of the problem is reduced by transforming the data into higher dimensions [44]. Again, we use the kernel package from Scikit-learn, choosing this time an rbf (radial basis function) kernel. We use the regularized loss and we also perform cross validation to tune the hyperparameter *alpha* that maximizes the bias-variance trade-off, which is more relevant in this case, owing to the higher descriptive power of the model.
3. A deep neural network (DNN). Thanks to the consistent number of free parameters, DNN is capable of detecting eventual huge non linearities and hidden patterns between the input data and the labels present in the physical problem. The advantages of implementing a DNN come at the expense of a much higher computational effort, necessary for training the DNN itself. To create our DNN we use Keras, a user-friendly front-end API for TensorFlow. The architecture of our DNN consists of an input layer with seven neurons (one for each thickness partition), an output layer with two neurons (one for each label: E* and Pcr), and five fully connected hidden layers. The first and last hidden layer has 32 neurons, while the three central layers have 64 neurons. For the activation function, we use the *relu* function for all the layers except the output one, where we implemented a *linear* activation function, commonly used in regression tasks. To minimize the loss function, we exploited the Adam optimization algorithm. To

properly train the DNN and its parameters, we run a total of 100 epochs with a batch size of 10.

For all three models the goodness of the fitting is evaluated with the R^2 score, which expresses the fraction of information reconstructed by the model. The three ML models analyzed in this study are built and run using Google Colab.

Results

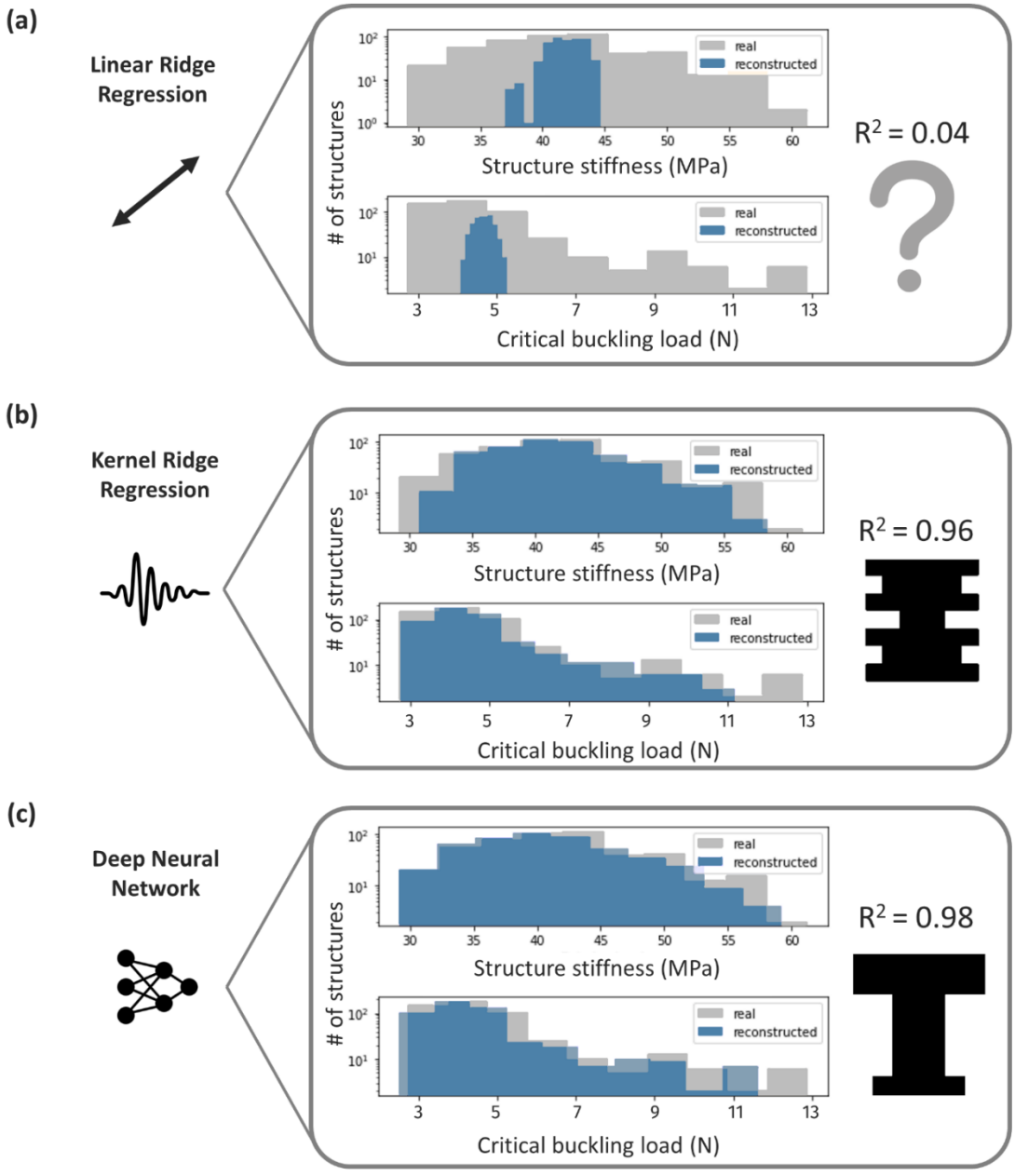

Figure 3 - Results of the three metamodels implemented: (a) Linear Ridge Regression, (b) Kernel Ridge Regression and (c) Deep Neural Network. In the figures are reported the distribution of the structure stiffness and critical buckling load together with the R^2 and the optimal structure predicted by the algorithm. It has to be noticed that the y-axis has logarithmic scale to highlight the differences between the calculated and predicted structures on the tails of the distribution.

Figure 3 shows the outcomes of our metamodels. The plots show the results in terms of structure stiffness and critical buckling load for the three adopted ML algorithms, together with the R^2 score. Note that the R^2 is calculated on the output vector, so it takes into account both the structure stiffness and the buckling load. Figure 3b,c also displays the optimal thickness distribution along the honeycomb cell wall predicted by the KRR and the DNN. The outcome of the simulations shows the potential of ML algorithms in terms of computational time with respect to the classic FE analysis approach. Computing 1000 different geometries in ANSYS takes approximately 3 hours of computational time, while to run the DNN, which is the most time-demanding implemented algorithm, it takes 75 seconds for the training and approximately one-tenth of a second to predict the behavior of 500 new structures; the same calculation by classic FE analysis requires 2 hours of CPU time, while using a ML approach the computational time was approximately 0.1 s, making ML algorithms ~10^5 faster than the FE method. This result is in line with previous studies, where different problems were addressed with a similar methodology. As we said before the FE simulations are run on a workstation, while the ML algorithms are run on Google Colab. However, even though we used different machines the computational time can be compared. In fact, from the author's experience Google Colab provides computing power similar to the workstation used for the FE simulations. This was assessed running the same script on both and comparing the computational time.
The plots in Figure 3a-c represent the number of different structures, of the validation test set, that have a specific value of K and P_{cr}. The grey shadow refers to the structure calculated via FE analysis while the blue shadow represents the structure predicted by the different ML algorithms. Note that all plot y-axes are in logarithmic scale. This makes it easier to see eventual differences on the tails, that with a linear scale will not be seen graphically.

Figure 3a shows the results for the linear regression model. As we can see the LRR has very poor performance. The LRR can only predict structures within a very narrow range of stiffness and critical stress that does not match the numerical simulations, meaning that the model is too simple to grasp the complexity of the analyzed phenomenon, where several non-linearities are present. Better results are obtained with the KRR(Figure 3b); the FE simulations and ML prediction distributions are much more overlapped, meaning that the metamodel predicts well the behavior of the simulated structure. Also, the R^2 score is good (R^2=0.963). However, the tails of the distributions are not well reconstructed, meaning that outlier's point can experience a distortion in their prediction, leading the algorithm not to being able to grasp their qualities. This is a crucial aspect in our study since we are particularly interested in the correct prediction of outliers. Indeed, our goal is to find structures that exhibit optimal physical properties, and such structures are far away from the mean of the labels' distribution. For this reason, it is mandatory for us that the algorithm, besides accurately predicting the overall behavior, is also able to precisely reconstruct the tails distribution. With DNN we are able to reach a very good representation of both the overall behavior and the tails (Figure 3c). This result can be inferred both graphically and from the R^2 value (R^2=0.983). Comparing the results of the KRR and the DNN they seem very similar in terms of accurate reconstruction of the overall behavior of the different structures; the R^2 scores are also very close, which further supports this outcome. However, the 2% increase in the R^2 score of the DNN is crucial. On the hand, this improvement leads to a better representation of the outliers, which are the best performing structures. On the other hand, it comes at the expense of a higher computational time required for the algorithm training. Due to its more complex architecture, DNN training time is 250 times higher than the KRR ($t_{train,DNN}$ = 75 s $t_{train,KRR}$ = 0.3 s). In our study, since the variables are few and the model is not extremely complex, this higher computational effort is justified by the fact that we are better at predicting the best-performing structures. However, this is an aspect that has to be evaluated when scaling to bigger datasets.

Comparing the performances of the optimal structures predicted by the DNN (Figure 3c) with those of the reference structure (i.e., the constant-thickness honeycomb), we can see that with our approach we reach a three-fold improvement in the structure stiffness (the analytical out of plane stiffness is about 23 MPa) and a four-fold improvement of the critical buckling stress (the analytical critical buckling stress is 2.6 MPa). Additional details are provided in the Supplementary Information.

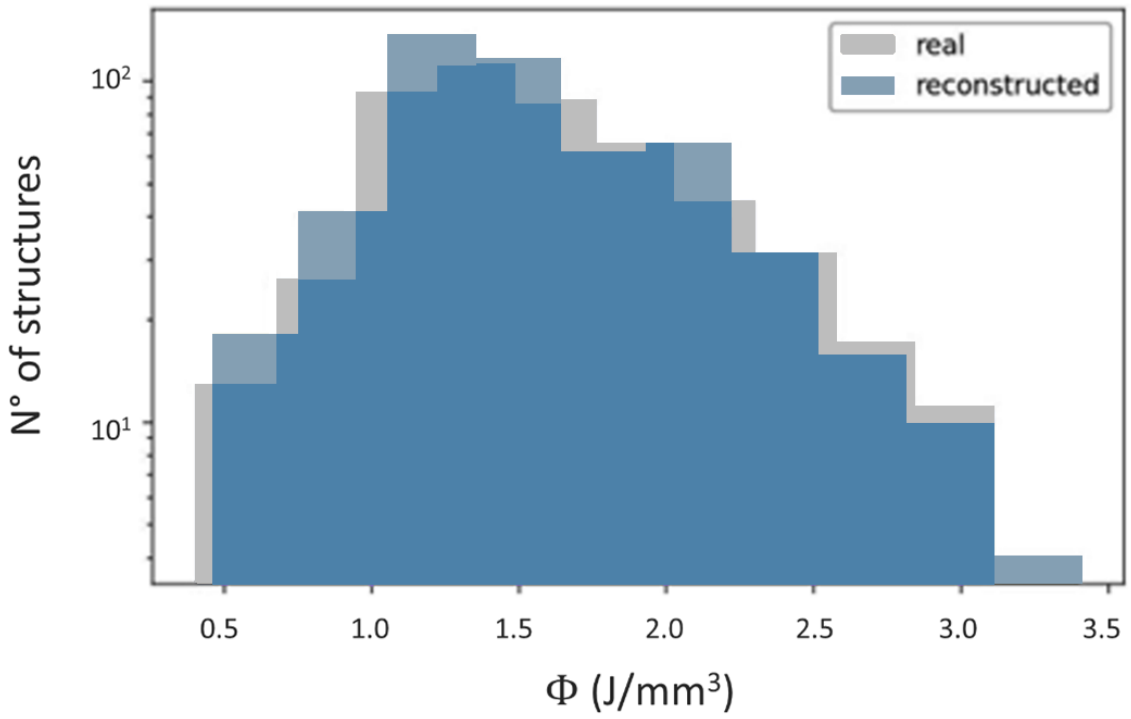

Figure 4 – Specific energy absorption distribution of structures calculated via FE analysis (grey) and the DDN ML algorithm (blue).

Also, as we would have expected, optimal honeycomb cells have a variable wall thickness along the out-of-plane direction. Similar results are reported in [ref], in which the authors demonstrated that tapered wall thickness honeycomb outperforms flat wall thickness honeycomb in energy absorption applications.

Figure 4 displays the results in terms of energy absorption, which is considered the parameter that combines the structure stiffness and critical buckling load, allowing a direct comparison among different structures. The results reported here are those obtained with the DNN. Again the y-axis is in logarithmic scale, and as we can see there is an extremely good prediction also on the tails. In the case of the absorbed energy, we get a 20-fold improvement with respect to the reference geometry (constant-thickness honeycomb).

Figure 5 shows the comparison between the natural structure thickness distribution and that predicted by the DNN. The structure predicted by the DNN shows a similar trend to the natural one: both structures show a thinner and cross-section in the central region and a thicker section at the top and the bottom. Clearly, the natural thickness distribution is much smoother, but this issue can be easily overcome by increasing the number of partitions in the honeycomb wall. This result is in line with what we were expecting, considering the theoretical behavior of thin structures under compression.

From the presented results we can clearly see the potential of the ML approach instead of the classic FE analysis. In fact, starting from a relatively small number of analyzed geometry we were able to exponentially expand the design space, finding the optimal thickness distribution that maximize the energy absorption capacity. Another important aspect is that the ML model takes into consideration not only the absorbed energy, but also the structure stiffness and the critical buckling load. This is important for two reasons: (i) forcing the model to fit also K and P_{cr} and not only the absorbed energy, we are forcing it create a function between the input and the output that try to describe the physical phenomenon; (ii) having as output from the FE and the ML algorithm K and P_{cr} we can have an immediate comparison with the analytical models, at least for the simpler geometries (i.e., the constant thickness wall unit cell). Also this approach demonstrated to be extremely flexible and modular, being adaptable at different and geometries, with different control parameters (i.e., stiffness, buckling load, absorbed energy, strength, etc), allowing the optimization of countless structures with respect to different parameters.

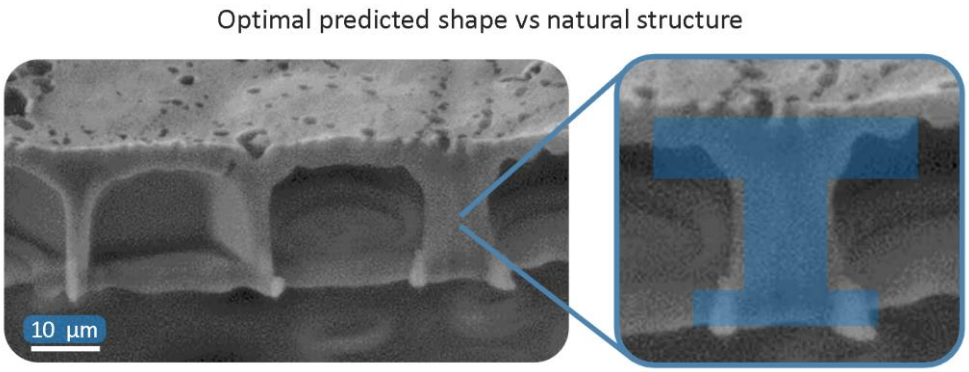

Figure 5 - Natural structure vs optimal predicted structure. Images modified from [39] *(CC BY 4.0).*

Conclusion

In this paper, we have developed an approach to design improved honeycomb structures for energy absorption application using an ML-based optimization technique. Three different ML algorithms, with different approaches are used: Linear Ridge Regression, Kernel Ridge Regression and Deep Neural Network. First of all, we create the geometries by defining a seven-dimensional vector describing the wall thickness distribution, while the 2D output vector describing the honeycomb performance in terms of structure stiffness and critical buckling load is calculated via FE simulation. The KRR and the DNN show good fitting on the data and are able to capture the non-linear behavior of the structure, while the linear model is too simple to describe the phenomenon. Indeed, the data regression-based metamodels allow one to: i) deepen the knowledge of the material design space, ii) find the optimum condition for a given application, and iii) tailor its properties to meet specific requirements for a chosen application, all in a fraction of time with respect to the classic FE analysis. To conclude the approach proposed in this work for the prediction of optimized energy absorption structures seems to be very promising for the definition of improved structure design with reduced computational effort, making ML algorithm more appealing for advanced material design than classical FE approaches.

References

[1] M. F. Ashby, "The properties of foams and lattices," *Philos. Trans. R. Soc. A Math. Phys. Eng. Sci.*, vol. 364, no. 1838, pp. 15–30, 2006, doi: 10.1098/rsta.2005.1678.

[2] T. A. Schaedler and W. B. Carter, "Architected Cellular Materials," *Annu. Rev. Mater. Res.*, vol. 46, pp. 187–210, 2016, doi: 10.1146/annurev-matsci-070115-031624.

[3] N. Kladovasilakis, K. Tsongas, D. Karalekas, and D. Tzetzis, "Architected Materials for Additive Manufacturing: A Comprehensive Review," *Materials (Basel).*, vol. 15, no. 17, pp. 1–18, 2022, doi: 10.3390/ma15175919.

[4] M. Osanov and J. K. Guest, "Topology Optimization for Architected Materials Design," *Annu. Rev. Mater. Res.*, vol. 46, pp. 211–233, 2016, doi: 10.1146/annurev-matsci-070115-031826.

[5] L. Musenich and F. Libonati, "Damage and Failure Mechanisms of Biological Materials," in *Reference Module in Materials Science and Materials Engineering*, Elsevier, 2022.

[6] J. F. V. Vincent, "Biomimetics - A review," *Proc. Inst. Mech. Eng. Part H J. Eng. Med.*, vol. 223, no. 8, pp. 919–939, 2009, doi: 10.1243/09544119JEIM561.

[7] P. Fratzl, "Biomimetic materials research: What can we really learn from nature's structural materials?," *J. R. Soc. Interface*, vol. 4, no. 15, pp. 637–642, 2007, doi: 10.1098/rsif.2007.0218.

[8] F. Libonati and M. J. Buehler, "Advanced Structural Materials by Bioinspiration," *Advanced Engineering Materials*, vol. 19, no. 5. 2017, doi: 10.1002/adem.201600787.

[9] T. Mead and S. Jeanrenaud, "The elephant in the room: Biomimetics and sustainability?," *Bioinspired, Biomim. Nanobiomaterials*, vol. 6, no. 2, pp. 113–121, 2016, doi: 10.1680/jbibn.16.00012.

[10] F. Barthelat, "Architectured materials in engineering and biology: Fabrication, structure, mechanics and performance," *Int. Mater. Rev.*, vol. 60, no. 8, pp. 413–430, 2015, doi: 10.1179/1743280415Y.0000000008.

[11] R. O. Ritchie, "The conflicts between strength and toughness," *Nat. Mater.*, vol. 10, no. 11, pp. 817–822, 2011, doi: 10.1038/nmat3115.

[12] M. Eder, S. Amini, and P. Fratzl, "Biological composites—complex structures for functional diversity," 2018. doi: 10.1126/science.aat8297.

[13] J. D. Marth, "A unified vision of the building blocks of life," *Nature Cell Biology*, vol. 10, no. 9. p. 1015, 2008, doi: 10.1038/ncb0908-1015.

[14] Z. Liu, Z. Zhang, and R. O. Ritchie, "Structural Orientation and Anisotropy in Biological Materials: Functional Designs and Mechanics," *Adv. Funct. Mater.*, vol. 30, no. 10, pp. 1–17, 2020, doi: 10.1002/adfm.201908121.

[15] W. Huang *et al.*, "Multiscale Toughening Mechanisms in Biological Materials and Bioinspired Designs," *Adv. Mater.*, vol. 31, no. 43, pp. 1–37, 2019, doi: 10.1002/adma.201901561.

[16] Z. Liu, M. A. Meyers, Z. Zhang, and R. O. Ritchie, "Functional gradients and heterogeneities in biological materials: Design principles, functions, and bioinspired applications," *Prog. Mater. Sci.*, vol. 88, pp. 467–498, 2017, doi: 10.1016/j.pmatsci.2017.04.013.

[17] S. E. Naleway, M. M. Porter, J. McKittrick, and M. A. Meyers, "Structural Design Elements in Biological Materials: Application to Bioinspiration," *Adv. Mater.*, vol. 27, no. 37, pp. 5455–5476, 2015, doi: 10.1002/adma.201502403.

[18] J. W. C. Dunlop, R. Weinkamer, and P. Fratzl, "Artful interfaces within biological materials," *Mater. Today*, vol. 14, no. 3, pp. 70–78, 2011, doi: 10.1016/S1369-7021(11)70056-6.

[19] J. Ren *et al.*, "Biological Material Interfaces as Inspiration for Mechanical and Optical Material Designs," 2019, doi: 10.1021/acs.chemrev.9b00416.

[20] T. Ackbarow and M. J. Buehler, "Hierarchical coexistence of universality and diversity controls robustness and multi-functionality in protein materials," *J. Comput. Theor. Nanosci.*, vol. 5, no. 7, pp. 1193–1204, 2008, doi: 10.1166/jctn.2008.2554.

[21] J. Harris, C. F. Böhm, and S. E. Wolf, "Universal structure motifs in biominerals: A lesson from nature for the efficient design of bioinspired functional materials," *Interface Focus*, vol. 7, no. 4, 2017, doi: 10.1098/rsfs.2016.0120.

[22] M. J. B. Steven W. Cranford, *Biomateriomics (Springer Series in Materials Science)*, 1st ed. Springer, Dordrecht, 2012.

[23] F. Libonati, G. X. Gu, Z. Qin, L. Vergani, and M. J. Buehler, "Bone-Inspired Materials by Design: Toughness Amplification Observed Using 3D Printing and Testing," *Adv. Eng. Mater.*, vol. 18, no. 8, pp. 1354–1363, 2016, doi: 10.1002/adem.201600143.

[24] U. G. K. Wegst, H. Bai, E. Saiz, A. P. Tomsia, and R. O. Ritchie, "Bioinspired structural materials," *Nat. Mater.*, vol. 14, no. 1, pp. 23–36, 2015, doi: 10.1038/nmat4089.

[25] E. D. Sanders, A. Pereira, and G. H. Paulino, "Optimal and continuous multilattice embedding," *Sci. Adv.*, vol. 7, no. 16, pp. 1–14, 2021, doi: 10.1126/sciadv.abf4838.

[26] L. R. Meza, A. J. Zelhofer, N. Clarke, A. J. Mateos, D. M. Kochmann, and J. R. Greer, “Resilient 3D hierarchical architected metamaterials,” *Proc. Natl. Acad. Sci. U. S. A.*, vol. 112, no. 37, pp. 11502–11507, 2015, doi: 10.1073/pnas.1509120112.

[27] L. Meng *et al.*, “From Topology Optimization Design to Additive Manufacturing: Today’s Success and Tomorrow’s Roadmap,” *Arch. Comput. Methods Eng.*, vol. 27, no. 3, pp. 805–830, 2020, doi: 10.1007/s11831-019-09331-1.

[28] H. Jiang, S. Mi, and J. Wan, “3D printing of carbon - based materials for supercapacitors,” *J. Mater. Res.*, 2021, doi: 10.1557/s43578-021-00323-1.

[29] A. Dijkshoorn, M. Schouten, G. Wolterink, R. Sanders, S. Stramigioli, and G. Krijnen, “Characterizing the Electrical Properties of Anisotropic, 3D-Printed Conductive Sheets for Sensor Applications,” *IEEE Sens. J.*, vol. 20, no. 23, pp. 14218–14227, 2020, doi: 10.1109/JSEN.2020.3007249.

[30] M. P. Bendsøe and O. Sigmund, *Topology Optimization*, vol. 5, no. 3. 2004.

[31] G. B. Olson, “Computational design of hierarchically structured materials,” *Science (80-.).*, vol. 277, no. 5330, pp. 1237–1242, 1997, doi: 10.1126/science.277.5330.1237.

[32] D. Morgan and R. Jacobs, “Opportunities and Challenges for Machine Learning in Materials Science,” *Annu. Rev. Mater. Res.*, vol. 50, pp. 71–103, 2020, doi: 10.1146/annurev-matsci-070218-010015.

[33] L. Himanen, A. Geurts, A. S. Foster, and P. Rinke, “Data-Driven Materials Science: Status, Challenges, and Perspectives,” *Adv. Sci.*, vol. 6, no. 21, 2019, doi: 10.1002/advs.201900808.

[34] K. Guo, Z. Yang, C. H. Yu, and M. J. Buehler, “Artificial intelligence and machine learning in design of mechanical materials,” *Mater. Horizons*, vol. 8, no. 4, pp. 1153–1172, 2021, doi: 10.1039/d0mh01451f.

[35] F. E. Bock, R. C. Aydin, C. J. Cyron, N. Huber, S. R. Kalidindi, and B. Klusemann, “A review of the application of machine learning and data mining approaches in continuum materials mechanics,” *Front. Mater.*, vol. 6, no. May, 2019, doi: 10.3389/fmats.2019.00110.

[36] C. T. Chen and G. X. Gu, “Machine learning for composite materials,” *MRS Commun.*, vol. 9, no. 2, pp. 556–566, 2019, doi: 10.1557/mrc.2019.32.

[37] A. Agrawal and A. Choudhary, “Deep materials informatics: Applications of deep learning in materials science,” *MRS Commun.*, vol. 9, no. 3, pp. 779–792, 2019, doi: 10.1557/mrc.2019.73.

[38] E. De Tommasi, J. Gielis, and A. Rogato, “Diatom Frustule Morphogenesis and Function: a Multidisciplinary Survey,” *Mar. Genomics*, vol. 35, no. 2017, pp. 1–18, 2017, doi: 10.1016/j.margen.2017.07.001.

[39] I. Zgłobicka *et al.*, “Insight into diatom frustule structures using various imaging techniques,” *Sci. Rep.*, vol. 11, no. 1, pp. 1–10, 2021, doi: 10.1038/s41598-021-94069-9.

[40] A. K. Noren, “Characterization of Structure and Optical Properties of Diatoms for improved Solar Cell Efficiency,” 2011.

[41] K. Li *et al.*, “Diatom-inspired multiscale mineralization of patterned protein-polysaccharide complex structures,” *Natl. Sci. Rev.*, vol. 8, no. 8, pp. 1–12, 2021, doi: 10.1093/nsr/nwaa191.

[42] Z. H. Aitken, S. Luo, S. N. Reynolds, C. Thaulow, and J. R. Greer, “Microstructure provides insights into evolutionary design and resilience of Coscinodiscus sp. frustule,” *Proc. Natl. Acad. Sci. U. S. A.*, vol. 113, no. 8, pp. 2017–2022, 2016, doi: 10.1073/pnas.1519790113.

[43] J. Schmidt, M. R. G. Marques, S. Botti, and M. A. L. Marques, “Recent advances and applications of machine learning in solid-state materials science,” *npj Comput. Mater.*, vol. 5, no. 1, 2019, doi: 10.1038/s41524-019-0221-0.

[44] T. J. Cleophas and A. H. Zwinderman, *Kernel Ridge Regression in Clinical Research*. 2022.